

CONTENTS

MRS-S Activities: Past, Present and Future

page 104...

MRS-S Executive Committee

page 105...

MRS-S Forthcoming Conference: ICMAT2007

page 105...

Highlights of previous MRS-S National Conferences

page 110...

Highlights of the Recent Literature

page 110...

Recent Books

page 112...

MRS-S Membership

page 113...

Materials Education & Research in Singapore

page 113...

Theme Article

page 114...

Forthcoming Conferences

page 132...

Contents of the Previous Issue

page 133...

Invitation to MRS-S Members

page 135...

➤ **MRS-S Activities: Past, Present and Future**

The Materials Research Society of Singapore (MRS-S) organized three International and two National Conferences in Singapore since 2001. The biennial "International Conference on Materials for Advanced Technologies (ICMAT)" series were held in 2001, 2003, and 2005. The biennial National Conferences were held in 2004 and 2006. MRS-S also sponsored/supported several other conferences, workshops, symposia, and public lectures. It instituted gold medals for the best outgoing students in Materials Science at the National University of Singapore and Nanyang Technological University. It recently instituted the "MRS Singapore Student Bursary Fund" at the National University of Singapore.

To reach out to the public, MRS-S has organized a number of public lectures by Nobel Laureates and also an astronaut.

MRS-S recently extended partial financial support to one Master Degree student of the Department of Materials Science and Engineering, National University of Singapore, to attend the GSAS Session on 'Advanced Solar Cell Research' in Taiwan. He also participated in the 'Project presentation competition' held during the Session.

MRS-S is pleased to learn that he came out successful in that competition, and was offered a fellowship to work on his proposed project in the near future at one of the prestigious Research Institutions in Taiwan, for an extended period of time.

The ICMAT-2007, to be held in Singapore during 1-6, July, 2007 will have 18 plus 5 Symposia, 9 Plenary, 3 Theme and 2 Public Lectures. There will also be an Exhibition comprising of Equipment Manufacturers, Book publishers and others who will display their products.

More than 2400 Abstracts have been received.

Details regarding the Plenary, Theme Lectures and the Symposia are presented in this Issue.

For additional information, see: <http://www.mrs.org.sg/conference/icmat2007/>

Schedule & Important Deadlines:

<i>Receipt of Manuscripts :</i>	01 May 2007
<i>(for the accepted Abstracts)</i>	
<i>Registration at Reduced Rates :</i>	15 April 2007
<i>Registration at Standard Rates :</i>	16 April to 15 June 2007
<i>Online Registration Closes :</i>	16 June 2007
<i>Registration at Onsite Rates :</i>	from 17 June 2007

➤ **Highlights of Previous ICMAT Conferences**

Year 2001 ♦ 1-6 July 2001	Year 2003 ♦ 7-12, Dec. 2003	Year 2005 ♦ 3-8, July 2005
16 Symposia	16 Symposia	25 Symposia
10 Plenary Lectures	9 Plenary Lectures	9 Plenary Lectures
4 Public Lectures by Nobel Laureates	2 Public Lectures by Nobel Laureates	2 Theme Lectures
1400 Delegates	1500 Delegates	3 Public Lectures by Nobel Laureates
18 Best Poster Awards	19 Best Poster Awards	2200 Delegates
36 Exhibitors	29 Exhibitors	28 Best Poster Awards
		43 Exhibitors

MRS-S Executive Committee

(For 2006–08)

President

B.V.R. Chowdari, NUS

Founding President

Shih Choon Fong, NUS

Vice Presidents

Lim Seh Chun, NUS

Freddy Boey, NTU

Secretary

Lam Yeng Ming, NTU

Joint Secretary

Chia Ching-Kean, IMRE

Treasurer

Ramam Akkipeddi, IMRE

Joint Treasurer

Feng Yuan Ping, NUS

Members

Ding Jun, NUS

Liu Ai Qun, NTU

Liu Bin, NUS

Lu Chun, IHPC

Patrick Poa Chun Hwa, IMRE

Shen Ze Xiang, NTU

G.V. Subba Rao, NUS

Teo Kie Leong, NUS

Tim White, NTU

J.J. Vittal, NUS

Honorary Auditors

Mike Loh, IMRE

Liu Zishun, NUS

NUS: National University of Singapore

NTU: Nanyang Technological University, Singapore

IMRE: Institute of Materials Research & Engineering, Singapore

IHPC: Institute of High Performance Computing, Singapore

MRS-S Forthcoming Conference

ICMAT 2007

International Conference on Materials for Advanced Technologies 2007 Incorporating GEM⁴ Conference on Cancer

1–6 July 2007, Singapore

Plenary Lectures (titles in italics)

Anthony K. CHEETHAM

International Center for Materials Research,
University of California, Santa Barbara, USA
*“Hybrid Inorganic-Organic Materials and Their
Applications”*

Claude COHEN-TANNOUJJI

Nobel Laureate in Physics, Laboratoire Kastler
Brossel, Département de Physique de l'ENS,
France
“Manipulating Atoms with Light”

Richard H. FRIEND

Cavendish Laboratory, University of Cambridge,
Cambridge, UK

H. Robert HORVITZ

Nobel Laureate in Physiology, Massachusetts
Institute of Technology, Cambridge, MA, USA
*“Cell Suicide: Programmed Cell Death in
Development and Disease”*

MRS-S OUTLOOK (ISSN 1793-3609) is published quarterly by the Materials Research Society of Singapore (MRS-S), c/o Institute of Materials Research & Engineering, 3, Research Link, Singapore 117 602.

Editor: G.V. Subba Rao. **Disclaimer:** Statements and opinions expressed in 'MRS-S OUTLOOK' are solely those of the authors, and do not reflect those of MRS-S, nor the editor and staff. **Permissions:** The subject matter contained in 'MRS-S OUTLOOK' can be freely reproduced for not-for-profit use by the readers; however, a word of acknowledgement will be appreciated.

Sumio IJIMA

Meijo University & AIST/Research Center for Advanced Carbon Material, Nagoya, Japan
"Nano-Carbon Materials: Their Fundamentals and Various Applications Including Nano-Biotechnology"

David LANE

Institute of Molecular and Cell Biology, Singapore
"Drug Discovery in the p53 Pathway"

K. Barry SHARPLESS

Nobel Laureate in Chemistry, The Scripps Research Institute (TSRI), California, USA

Subra SURESH

Massachusetts Institute of Technology, USA
"Nanotechnology and Materials Science at the Intersections of Engineering, Biology and Medicine"

R. Stanley WILLIAMS

Hewlett-Packard Laboratories, USA
"Computing at the Nanoscale will Employ Different Physics and Logic Operations"

Theme Lectures (titles in italics)**Martin JANSEN**

Max-Planck Institute for Solid State Research, Stuttgart, Germany
"Synthesis Planning in Solid State and Materials Chemistry"

S. MOHAN

Indian Institute of Science, Bangalore, India
"Role of Multidisciplinary Materials Research in Technology Creation and Commercialisation"

Pankaj VADGAMA

IRC in Biomedical Materials, Queen Mary, University of London, UK
"Designer Surfaces for the Biological Interface — How Far Can We Enhance Functional Performance?"

Symposia Details

Symposium A Advanced Functional Biomaterials

Chair: YANG Yi-Yan *Institute of Bioengineering and Nanotechnology, 31 Biopolis Way, The Nanos, #04-01, Singapore 138669. Tel: (65) 6824 7106, Fax: (65) 6478 9084, Email: yyyang@ibn.a-star.edu.sg*

Keynote Speakers: 5; Invited Speakers: 14

Symposium B Developing Nano-Bio Interface

Chair: LOH Kian Ping *National University of Singapore, Department of Chemistry, 3 Science Drive 3, Singapore 117543. Tel: (65) 6516 4402, Fax: (65) 6779 1691, Email: chmlohkp@nus.edu.sg*

Keynote Speakers: 5; Invited Speakers: 21

Symposium C Biofunctional Materials: From Understanding to Design

Chair: LIU Xiang Yang *National University of Singapore, Department of Physics, 2 Science Drive 3, Singapore 117542. Tel: (65) 6516 2812, Fax: (65) 6777 6126, Email: phyliuxy@nus.edu.sg*

Invited Speakers: 18

Symposium D Semiconductor Photonics: Nanostructured Materials and Devices

Chair: CHUA Soo Jin *Institute of Materials Research and Engineering, 3 Research Link, Singapore 117602. Tel: (65) 6874 8377, Fax: (65) 6872 0785, Email: elecjs@nus.edu.sg*

Invited Speakers: 16

Symposium E Nanodevices and Nanofabrication

Chair: ZHOU Wei *Nanyang Technological University, Singapore Precision Engineering & Nanotechnology Centre, 50 Nanyang Avenue, Singapore 639798. Tel: (65) 6790 4700, Fax: (65) 6791 1859, Email: MWZhou@ntu.edu.sg*

Invited Speakers: 16

Symposium F Microstructured and Nanostructured Optical Fibers

Chair: SHUM Ping *Nanyang Technological University, Singapore Network Technology Research Centre, Research Techno Plaza, 50 Nanyang Drive, Singapore 637553. Tel: (65) 6790 4217, Fax: (65) 6792 6894, Email: epshum@ntu.edu.sg*

Invited Speakers: 15

Symposium G Scanning Probe Microscopy in Materials Research

Chair: N. CHANDRASEKHAR *Institute of Materials Research and Engineering, 3 Research Link, Singapore 117602. Tel: (65) 6874 8586, Fax: (65) 6774 4657, Email: n-chandra@imre.a-star.edu.sg, phycn@nus.edu.sg*

Keynote Speakers: 6; Invited Speakers: 20

Symposium H MEMS Technology and Devices

Chairs: LIU Ai-Qun *Nanyang Technological University, School of Electrical & Electronic Engineering, 50 Nanyang Avenue, Singapore 639798. Tel: (65) 6790 4336, Fax: (65) 6792 0415, Email: eaqliu@ntu.edu.sg*
LU Chun *Institute of High Performance Computing, Singapore*

Keynote Speakers: 6; Invited Speakers: 2

Symposium J Materials for Advanced Sensors and Detectors

Chair: Girish M. KALE *University of Leeds, Leeds LS2 9JT, United Kingdom. Tel: (44) 113 3432805, Fax: (44) 113 3432384, Email: g.m.kale@leeds.ac.uk*

Keynote Speakers: 4; Invited Speakers: 34

Symposium K Nanostructured and Bulk Materials for Electrochemical Power Sources^a

Chair: S.R.S. PRABAHARAN *The University of Nottingham, Faculty of Engineering and Computer Science, The University of Nottingham Malaysia Campus (UNMC), Jalan Broga, 43500 Semenyih, Selangor, Malaysia. Tel: (603) 8924 8125, Fax: (603) 8924 8017, Email: prabaharan.sahaya@nottingham.edu.my*

Keynote Speakers: 3; Invited Speakers: 31

Symposium L Catalytic Materials and Technologies for a Sustainable Economy

Chair: Stephan JAENICKE *National University of Singapore, 3 Science Drive 3, Singapore 117543. Tel: (65) 6516 2918, Fax: (65) 6779 1691, Email: chmsj@nus.edu.sg*

Keynote Speakers: 7; Invited Speakers: 9

Symposium M New Routes to Inorganic Materials, Films, and Nanocrystals

Chair: Jagadese J. VITTAL *National University of Singapore, Department of Chemistry, 3 Science Drive 3, Singapore 117543. Tel: (65) 6516 2975, Fax: (65) 6779 1691, Email: chmjjo@nus.edu.sg*

Keynote Speakers: 17; Invited Speakers: 13

Symposium N Synchrotron Radiation for Making and Measuring Materials

Chair: Herbert O. MOSER *Singapore Synchrotron Light Source, Singapore. E-mail: slsmm@nus.edu.sg*

Keynote Speakers: 3; Invited Speakers: 16

Symposium O Frontiers in Computational Materials Science

Chair: FENG Yuan Ping *National University of Singapore, 2 Science Drive 3, Singapore 117542. Tel: (65) 6516 2960, Fax: (65) 6777 6126, Email: phyfyp@nus.edu.sg*

Keynote Speakers: 3 ; Invited Speakers: 37

Symposium P Electromagnetic Materials

Chair: LIM Hock *National University of Singapore, Singapore. E-mail: tslganyb@nus.edu.sg*

Invited Speakers: 11

Symposium Q Advanced Structural and Functional Materials for Protection

Chairs: SHANG Huai Min *Nanyang Technological University, Singapore*

William LAU *Defence Science & Technology Agency, Singapore. E-mail: miiytok@ntu.edu.sg*

Keynote Speakers: 9; Invited Speakers: 3

^aThis symposium is partially sponsored by Valence Technology Inc., USA.

**Symposium R Polymer and Molecular Electronics: Chemistry,
Physics & Materials Science**

Chairs: **Hardy CHAN** *National University of Singapore, Department of Chemistry, 3 Science Drive 3, Singapore 117543. Tel: (65) 6516 2673, Fax: (65) 6777 1691, Email: chmcs@nus.edu.sg*

Freddy BOEY *Nanyang Technological University, Singapore*

Keynote Speakers: 9; Invited Speakers: 6

Symposium S Education in Nanoscience and Nanoengineering

Chair: **Vincent TAN** *National University of Singapore, Singapore. E-mail: kellylow@nus.edu.sg*

Keynote Speakers: 1; Invited Speakers: 8

GEM⁴ Conference on Cancer — Thematic Symposia

(1) NANOTECHNOLOGY & BIOPHYSICAL ASSAYS AND CANCER DIAGNOSTICS

Local Chairpersons Nanotechnology:

Si-Shen Feng *National University of Singapore. Email: biefss@nus.edu.sg*

Chwee Teck Lim *National University of Singapore. Email: bielimct@nus.edu.sg*

Gene Expression Signatures:

Lance Miller *Genome Institute of Singapore. Email: millerL@gis.a-star.edu.sg*

Molecular Diagnostics:

Manuel Salto-Tellez *National University of Singapore. Email: patmst@nus.edu.sg*

International Chairperson:

Dr Joseph R. Nevins *DUMC*

(2) BIOIMAGING OF CANCER

Local Chairperson:

WANG Shih-Chang *FRANZCR, National University of Singapore, Singapore. Email: dnrwsc@nus.edu.sg*

International Chairpersons:

NIE Shuming *Emory University and Georgia Institute of Technology, USA. Email: snie@emory.edu*

Murali KRISHNA *Chief, Biophysical Spectroscopy Section, National Institute of Health, USA*

**(3) COMPUTATIONAL SYSTEMS BIOLOGY AND MOLECULAR EPIDEMIOLOGY OF
CANCER**

Local Chairperson:

Guillaume BOURQUE *Genome Institute of Singapore, Singapore. Email: bourque@gis.a-star.edu.sg*

International Chairperson:

Edision LIU *Genome Institute of Singapore, Singapore. Email: liue@gis.a-star.edu.sg*

(4) NOVEL BIOMATERIALS FOR DRUG DELIVERY; SURGICAL INTERVENTION & ROBOTICS; TUMOR IMMUNOLOGY*Symposium details to be confirmed***(5) CANCER CELL INTERACTION, MOTILITY AND METASTASIS***Local Chairperson:***J.P. THIERY** *Institute of Molecular & Cell Biology, A*STAR, Singapore. Email: jpthiery@imcb.a-star.edu.sg**International Chairpersons:***Benny Geiger** *Weizmann Institute of Science, Israel***Joachim P. Spatz** *Max-Planck-Institute for Metals Research & University of Heidelberg, Germany***Highlights of previous MRS-S National Conferences****Year 2004 (6 August 2004)**

- 20 Invited Talks • 130 Poster Papers
- 4 Best Poster Awards

Year 2006 (18–20 January 2006)

- Includes the Symposium on 'Physics and Mechanics of Advanced Materials'
- 60 Invited Talks • 200 Poster Papers • 1 Public Lecture • 5 Best Poster Awards

Highlights of the Recent Literature*(Contributed by the Editor)***The Future of Energy Supply: Challenges and Opportunities**

A timely essay on the available renewable and non-renewable energy sources, with 67 references most of them being recent, is presented by Armaroli and Balzani [1]. The present status and prospects of fossil fuels (oil, natural gas, and coal), nuclear (fission and fusion), hydroelectric, biomass, bio-diesel, solar, wind, tidal, and geothermal energy sources have been reviewed. A strong case has been made for the progressive

reduction in the burning of fossil fuels to supply the energy needs of the world community, and prompt global action to develop and adopt several of the renewable energy sources. In the words of the authors, "solving the energy problem is indeed a great question that needs to be tackled by an interdisciplinary scientific effort".

References

- [1] N. Armaroli and V. Balzani (2006). **Angew. Chem. Int. Ed.** 46(1–2): 52–66.

Photoconductive Coaxial Nanotubes of Molecularly Connected Electron Donor and Acceptor Layers

Formation by self-assembly and photoconduction properties of coaxial nanotubes with 16 nm diameter and several micrometers long, consisting of electron-donating π -stacked layers of the molecules of hexabenzocoronene (HBC) and laminated by the electron-accepting molecules of trinitrofluorenone (TNF) have been reported by Yamamoto *et al* [1]. The nanotubes exhibited a large photocurrent upon irradiation: when irradiated with light of wavelength, $\lambda = 300$ – 650 nm at a power density, 70 mW mm^{-2} , at an applied voltage of $+2 \text{ V}$, the photocurrent and darkcurrent of the nanotubes were 4.2 nA and 0.07 pA , respectively. As the power density of the incident light was increased from 3.4 to 150 mW mm^{-2} , the observed photocurrent linearly increased. Further, the photocurrent was found to be nearly proportional to the applied voltage, ranging from -2 to $+2 \text{ V}$, indicating an ohmic behavior of the electrical conduction. It is pointed out that the photoexcitation of the self-assembled HBC should result in the generation of a charge-separated state involving radical cations and anions in the inner and outer layers (consisting of TNF molecules) of the nanotubes, respectively. Such a spatial separation of the charge-carriers would prevent a rapid recombination, thereby enabling the photoconduction along the nanotubes. The authors suggest that such a coaxial donor–acceptor configuration of the nanotubes is highly attractive for optoelectronic applications.

It must be mentioned, however, that the formation of the self-assembled coaxial nanotubes was found to be dependent on the concentration of the reactants in the solution, and diffusion of methanol vapor. Yellow-colored nanotubes formed only at low concentrations (0.12 mM of HBC–TNF dissolved in the solvent, tetrahydrofuran), whereas at higher concentrations (1.2 mM) brown-colored microfibers composed of HBC–TNF charge-transfer complexes formed. The latter showed a different morphology, structure, and

spectral properties, and hardly exhibited photocurrent generation.

References

- [1] Y. Yamamoto, T. Fukushima, Y. Suna, N. Ishii, A. Saeki, S. Seki, S. Tagawa, M. Taniguchi, T. Kawai and T. Aida (2006). *Science* 314: 1761–1764 (Dec., 15 Issue).

Patterning Organic Single-Crystal Transistor Arrays

Briseno *et al* [1] recently described a method for fabricating large arrays of single-crystals of a wide range of organic semiconductors (e.g., rubrene, pentacene, anthracene, C_{60} , fluorinated copper phthalocyanine, tetracyanoquinodimethane) directly on to the electrodes, constituting the source and drain connections. The substrates used were Si/SiO₂ surfaces or flexible plastic. To promote local crystal nucleation during the growth by the vapor transport method, the substrate was “stamped” with a film of octadecyltriethoxysilane (OTS) using a polydimethylsiloxane (PDMS) stamp with a relief structure in the desired pattern. Results on the large arrays (14×14 source–drain electrode arrays and channel lengths of 10 , 20 , 50 , and $100 \mu\text{m}$) of high-performance organic single-crystal field-effect transistors with mobilities as high as $2.4 \text{ cm}^2 \text{ V}^{-1} \text{ s}^{-1}$ and on–off ratios greater than 10^7 (in the case of rubrene) on Si/SiO₂ surface, and on the devices consisting of single-crystals of rubrene on flexible substrates that retain their performance after significant bending, have been presented.

More work is needed, however, to turn the above technique into a viable organic semiconductor technology. In particular, the orientation and alignment of the single-crystals, the reproducibility and control of the quality of the electrical contact between the semiconductor and the dielectric layer, as well as between the semiconductor and the electrodes need to be carefully studied and optimized. Nevertheless, the work

represents a significant step toward the realization of large-area organic semiconductor electronics for display and other applications.

References

- [1] A.L. Briseno, S.C.B. Mannsfeld, M.M. Ling, S. Liu, R.J. Tseng, C. Rees, M.E. Roberts, Y. Yang, F. Wudl and Z. Bao (2006). *Nature* 444: 913–917 (Dec., 14 Issue).

Spintronics: A Challenge for Materials Science and Solid-State Chemistry

The current status of materials research in the field of spin electronics (spintronics) and the related area of magnetoelectronics has been reviewed by Felser *et al.* [1]. Spintronics makes use of both charge and spin of electrons (or

holes) for the devices like “spin valves”. Magnetoelectronics deals with devices employing ferromagnetic metals or semiconductors. In the review, materials exhibiting giant- and colossal-magnetoresistance, and half-metallic ferromagnetism, including ferromagnetic semiconductor behavior, have been discussed. “True” ferromagnetic semiconductors with Curie temperatures higher than the ambient one are not yet known. In the words of the authors, “the design of new materials for spintronics remains a challenge for solid-state chemistry”.

References

- [1] C. Felser, G.H. Fecher and B. Balke (2007). *Angew. Chem. Int. Ed.* 46: 668–699.

Recent Books in the Area of Materials Science, Engineering and Technology

(Contributed by the Editor)

Carbon-Rich Compounds: From Molecules to Materials. Edited by Michael Haley and Rik R. Tykwinski, Wiley-VCH, Weinheim, 2006, 643 pp., Hardcover, ISBN 978-3-527-31224-2, €159.00.

For a review, see *Angew. Chem. Int. Ed.* **46(4)**, 491–492 (2007).

Photorefractive Materials: Fundamental Concepts, Holographic Recording and Materials Characterization. By Jaime Frejlich, 1st Edition, Wiley-VCH, (2006) Hardcover, ISBN-13: 978-0-471-74866-3 / ISBN-10: 0-471-74866-8, 309 pp., €105.

Nanomaterials for Biosensors, Edited by Kumar, S.S.R. Challa (Nanotechnologies for the

Life Sciences, 1st Edition, Wiley-VCH, 2006), Vol. XXI, 409 pp., Hardcover, ISBN-13: 978-3-527-31388-4 / ISBN-10: 3-527-31388-5. €139.

Hybrid Materials: Synthesis, Characterization, and Applications. Edited by Guido, Kickelbick, 1st Edition, Wiley-VCH, 2006, Vol. XVIII, 498 pp., Hardcover, ISBN-13: 978-3-527-31299-3 / ISBN-10: 3-527-31299-4, €149. – Handbook/Reference Book.

Functional Organic Materials: Syntheses, Strategies and Applications. Edited by Müller, J.J. Thomas and Bunz, H.F. Uwe, 1st Edition, Wiley-VCH, 2006, Vol. XX, 592 pp., Hardcover, ISBN-13: 978-3-527-31302-0 / ISBN-10: 3-527-31302-8, €249. – Handbook/Reference Book.

MRS-S Membership

Readers are invited to become members of the Materials Research Society of Singapore (MRS-S).

Professional Membership is open to any person engaged in activities associated with materials science, engineering and technology.

Student Membership is open to any bonafide student of a tertiary institution genuinely interested in the practice of materials science, engineering and technology.

Corporate Membership is open to any organisation, government or private, commercial or otherwise, that is in any way engaged in any activities that deal with any aspect of material science, engineering and technology. A Corporate Membership is entitled to nominate two of its employees as its official representatives and to change its nominees from time to time provided the Committee has no objection to any such nomination.

Annual Subscription Fee:

Professional Membership: S\$50

Student Membership: S\$5

Corporate Membership: S\$500

For details and application form, please visit: www.mrs.org.sg

Materials Education & Research in Singapore

There are two Universities and several Research Institutes in Singapore involved in teaching, research and development in the broad area of Materials Science, Engineering and Technology. These are listed below along with the Websites and provide information on the available courses and opportunities for undergraduate, graduate and post doctoral research. They also entertain queries regarding openings for Research Scientists and Faculty positions.

National University of Singapore: www.nus.edu.sg

Nanyang Technological University: www.ntu.edu.sg

Institute of Materials Research and Engineering (IMRE): www.imre.a-star.edu.sg

Institute of Microelectronics (IME): www.ime.a-star.edu.sg

Data Storage Institute: www.dsi.a-star.edu.sg

Institute of Chemical & Engineering Sciences: www.ices.a-star.edu.sg

Institute of High Performance Computing: www.ihpc.a-star.edu.sg

Singapore Institute of Manufacturing Technology: www.SIMTech.a-star.edu.sg

Institute of Bioengineering and Nanotechnology (IBN): www.ibn.a-star.edu.sg

About the Theme Article Authors



Dr. Wang Chenchen, B. Eng. (Hons), Ph.D.

Department of Electrical & Computer Engineering,
Faculty of Engineering,
National University of Singapore,
4 Engineering Drive 3, Singapore 117576
Email: wcc19@yahoo.com

Dr. Wang graduated in 2002 from National University of Singapore (NUS) with first class honors in engineering. He obtained his Ph.D. degree in electrical and computer engineering department of NUS in 2006. His Ph.D. research was focused on the magnetic and spin-dependent transport properties in artificially engineered antidot mesostructures. During Dr. Wang's Ph.D. training, he developed expertise in micron- and nano-fabrication such as UV and electron beam lithography, as well as in electrical and magnetic characterization tech-

niques such as magnetic force microscopy, vibrating sample magnetometer, magnetoresistance, and cryogenic measurements.

In 2005, Dr. Wang was awarded Singapore Millennium Foundation Fellowship and he worked as a research officer and later became a research fellow after his Ph.D. conferment under Prof. Adekunle Adeyeye till present. His current research interest is field-coupled logic, spin-dependent transport in ferromagnetic nanostructures, and high resolution magneto-optics.



Mr. Navab Singh, M. Sc. (Phys), M. Tech.

Institute of Microelectronics,
11 Science Park Road,
Singapore Science Park II, Singapore 117685
E-mail: navab@ime.a-star.edu.sg

Navab Singh is a Member of Technical Staff with the Institute of Microelectronics (IME), Singapore. He graduated in physics with a first class from the Meerut University, India, in 1992. He obtained his M.Tech. degree in solid state materials from Department of Physics at Indian Institute of Technology, Delhi, India, in 1995. His current research area is nanowire CMOS technology with expertise in DUV lithography. He is also pursuing Ph.D. in the area of nanomagnetism at Electrical and Computer Engineering, National University of Singapore (NUS).

Prior to joining IME, he worked as a Photolithography Engineer with TECH Semiconductor Pte. Ltd., Singapore, from August 1999 to June 2001, and with SITAR, Bangalore, India, from March 1996 to July 1999. He has been a Lecturer in Physics with DPBS (PG) College, Anupshahr, India, from December 1992 to May 1994. Navab Singh has authored or coauthored more than 75 papers in reviewed journals and conferences. His work on Si, SiGe nanowire CMOS devices was selected for preconference publicity for IEDM 2006.

Theme Article

Spin Engineering: Ferromagnetic Antidot MesostructuresC. C. Wang¹, N. Singh^{1,2} and A. O. Adeyeye¹¹Department of Electrical and Computer Engineering, National University of Singapore, Singapore²Institute of Microelectronics, Singapore**1 Introduction**

In the last decade, there has been significant interest in the properties of magnetic mesostructures with lateral dimensions in the micron to nanoscale range, both from fundamental and application viewpoints. Fundamentally, novel properties emerge as the lateral size of the magnets becomes comparable to or smaller than certain characteristic length scales, such as spin diffusion length and magnetic domain wall width. For low dimensional magnetic structures, the spin configuration and switching process are very sensitive to shape variation and edge roughness because of the spatially varying demagnetizing field. There have been many studies on magnetic mesostructures and nanostructures, including magnetic wires [1,2], dots [3–5], and rings [6,7]. Interesting and novel properties have been observed due to modified spin configurations resulting from the reduction of the lateral dimensions.

From a technological viewpoint, magnetic meso- and nanostructures form the basic building blocks for various potential spintronic applications. In data storage applications, as the recording media rapidly approach the superparamagnetic limit (whereby stored information is unstable due to thermal fluctuation), patterned media consisting of arrays of single domain nanomagnets have been proposed as a candidate for recording density up to 1 Terabit/in² [8,9]. Another application of magnetic mesostructures is in magnetic random access memory, which has various advantages over conventional memories such as high speed, high density, and nonvolatility [10]. Magnetic nanostructures are also being explored in logic applications [11–14]. The concept of novel logic devices incorporating

nanomagnets has been validated with submicron ferromagnetic dots, which demonstrate the data-manipulation capability of arrays of interacting elements [11,14].

Another class of magnetic mesostructures, which have been receiving increasing attention lately, is the so-called antidot structures. Antidot structures are the reverse of isolated mesostructures in which arrays of holes (antidots) are embedded into contiguous magnetic materials. The antidots can be described as artificially engineered “defects” in an otherwise continuous film. The question of how these defects affect the macroscopic and microscopic magnetic properties of the continuous media is of great interest, and the switching mechanism during the magnetization reversal process is an important issue that is still being studied rigorously. With the advances in nanofabrication and other controlled fabrication techniques, it is possible to create well-controlled antidot structures in thin magnetic films. It has been found that the antidots can “harden” the magnetic thin film by pinning of the magnetic domain walls [15]. The size and distribution of the engineered holes can greatly influence the properties of the film such as the coercive field, magnetic anisotropy, and magnetization reversal behavior [16–18]. Microscopically, the presence of ordered holes could also modify the intrinsic magnetic anisotropy of the film locally, inducing well-defined periodic domain structures in the vicinity of the holes [19–21].

In this theme article, we present a systematic study of the magnetic and spin-dependent transport properties of lithographically defined antidot mesostructures using a combination of characterization techniques and simulation tools. We start this article with a review of the effect

of nonmagnetic inclusions in bulk magnetic materials, which is followed by the fabrication and characterization techniques used for studying the antidot structures. We later investigated in detail the magnetization reversal process in the $\text{Ni}_{80}\text{Fe}_{20}$ antidot arrays using magnetoresistance (MR) measurements, and found that the reversal properties of the continuous film can be markedly modified by the presence of antidot arrays. Subsequently, we show that the magnetic anisotropy of the ferromagnetic thin film can be systematically tailored by changing the antidot lattice geometry. The microscopic origin responsible for the anisotropy distribution was elucidated by micromagnetic simulations of remanent spin states. Lastly, we study the magnetic and transport properties of multilayer antidot nanostructures, which consist of $\text{Ni}_{80}\text{Fe}_{20}$ and Co ferromagnetic layers separated by a Cu spacer layer. It was observed that the magnetic coupling and transport mechanisms are markedly dependent on the spacer layer thickness.

2 Background

The study of the effect of defects in the ferromagnetic materials can be traced back to early last century, when researchers were trying to

understand the origin of coercivity exhibited by the magnetic materials. It is now clear that the existence of imperfections, such as grain boundaries, precipitates, inclusions, and surface roughness, can lower the domain wall energy at a particular position in the material, or they can repel the continual domain wall motion by placing a barrier in front of the wall [22]. This hindrance to the domain wall propagation, or the so-called domain wall pinning, is responsible for the coercivity in soft magnetic materials, and is one of the sources of the well-known Barkhausen jumps [23].

The in-depth theoretical study of the domain wall pinning effect was first initiated by Kersten, who suggested the inclusion theory [24]. The pinning effect was explained by considering the lowering of the net wall "volume" (energy). When the wall contains a spherical inclusion, as illustrated in Fig. 1(a) and (b), the reduction in wall energy (E_w) can be shown as

$$E_w = \gamma\pi r^2, \quad (1)$$

where γ is the wall energy density for a nonmagnetic inclusion with radius r .

Néel [25] later found that free poles on an inclusion could be a far greater source of energy. An inclusion entirely within a domain, as shown

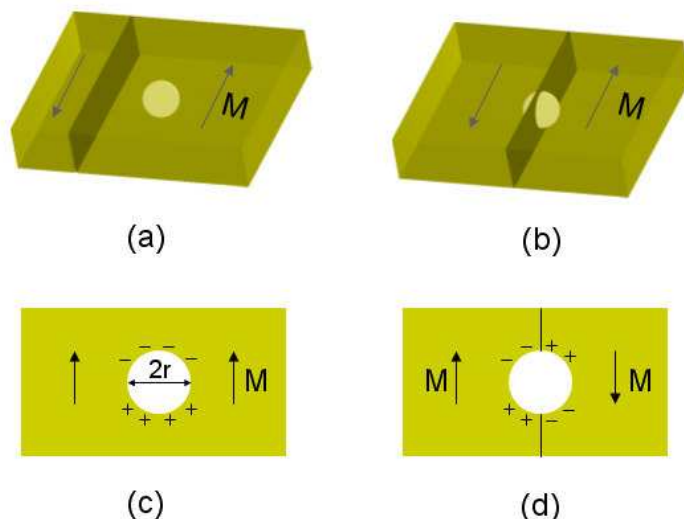


Fig. 1. (a) and (b) A schematic illustration of a moving domain wall before intersecting a nonmagnetic inclusion and resting on the inclusion, respectively. (c) and (d) The surface charge distribution before and after the intersection of the wall with the inclusion.

in Fig. 1(c), has free poles on it and an associated magnetostatic energy (E_m) of

$$E_m = \frac{8\pi^2 M_s^2 r^3}{9}, \quad (2)$$

where M_s is the saturation magnetization of the material. When the wall bisects the inclusion as shown in Fig. 1(d), the poles are redistributed and the magnetostatic energy is approximately halved.

If we compare the two mechanisms by taking the ratio of the energy reduction by the free-pole effect to the wall-area effect, it can be shown that the ratio

$$X = \frac{E_w}{E_m} = \frac{4\pi M_s^2 r}{9\gamma} \quad (3)$$

is proportional to the radius of the inclusion. This implies that the magnetostatic energy becomes the dominant source of energy reduction for larger inclusion size.

It was also pointed out by Néel that the magnetostatic energy of an inclusion in a domain could be further decreased by subsidiary spike domains formed on the inclusion, and the domain wall pinning could be a result of the subsidiary domains interacting with the moving domain wall, as shown in Fig. 2(a) and (b). The experimental observation of the spike domain was later reported by Williams [26], and a two-spike domain was observed as sketched in Fig. 2(c). In real magnetic materials, the defects are randomly distributed and each domain wall is intersected by a number of them. The domain wall pinning introduced by the collection of these isolated inclusions is responsible for an increase of

the coercivity in soft ferromagnetic materials.

In contrast to the nonmagnetic inclusions commonly studied in bulk materials, the lithographically defined antidot arrays are usually well ordered and highly symmetric. The volume density of the antidots can also be precisely controlled even in the regime of densely packed structures, such as those to be studied in this article. In most of the studies, it has been found that the presence of antidots exhibits a much more enhanced effect in modifying the properties of thin ferromagnetic films than the randomly distributed intrinsic defects do to bulk materials [27–29].

3 Experimental Processes

The processes involved in fabricating the ordered antidot mesostructures in this article are through the top-down approach, which is based on the idea of patterning on a large scale and reducing the lateral dimensions using lithography techniques. A typical flow of fabrication process is illustrated in Fig. 3, which can be generally divided into five steps, namely wafer cleaning, resist coating, lithography and resist development, deposition, and liftoff.

In our experiments, large-area $\text{Ni}_{80}\text{Fe}_{20}$ antidot structures ($4 \times 4 \text{ mm}^2$) were fabricated on commercially available silicon substrate using advanced KrF photolithography at 248 nm exposing wavelength. To create patterns in the resist, the substrate was coated with a 60 nm thick antireflective layer followed by a 480 nm positive

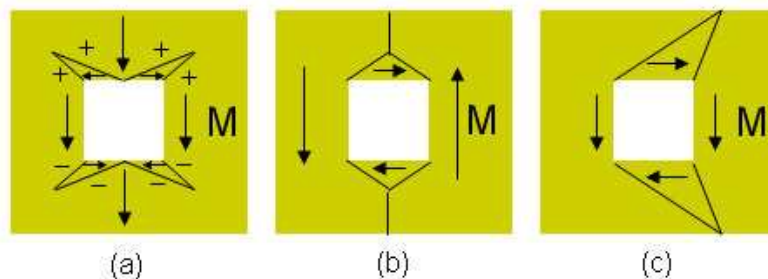


Fig. 2. (a) and (b) Spike domain and closure domain on an inclusion as suggested by Néel. (c) A two-blade spike domain observed experimentally by Williams.

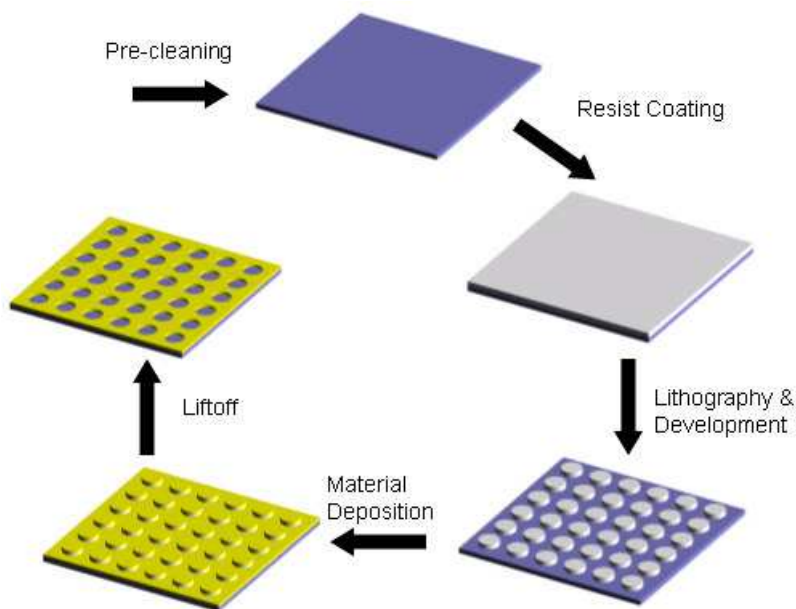


Fig. 3. A typical flow of fabrication process for an antidot sample.

Deep UV (DUV) photoresist. A Nikon lithographic scanner with KrF excimer laser radiation was used in exposing the resist. The antidot pitch on the mask was kept at 450 nm. Details of the fabrication process are described in [30]. Shown in Fig. 4(a) is the atomic force micrograph of the resist profile for the antidot arrays.

To convert the resist patterns into antidots, ferromagnetic material $\text{Ni}_{80}\text{Fe}_{20}$ was deposited using e-beam evaporation. The pressure was maintained at 2×10^{-6} Torr during deposition.

Liftoff of the deposited film was carried out in isopropyl alcohol. Completion of the liftoff process was determined by the color contrast of the patterned $\text{Ni}_{80}\text{Fe}_{20}$ area. The final structure consists of $\text{Ni}_{80}\text{Fe}_{20}$ arrays of closely packed circular antidots with diameter 300 nm and center-to-center spacing of 450 nm, as shown in Fig. 4(b).

To probe the transport properties of the fabricated antidot array structures, electrical contacts were made on the pattern using standard optical lithography, metallization, and liftoff

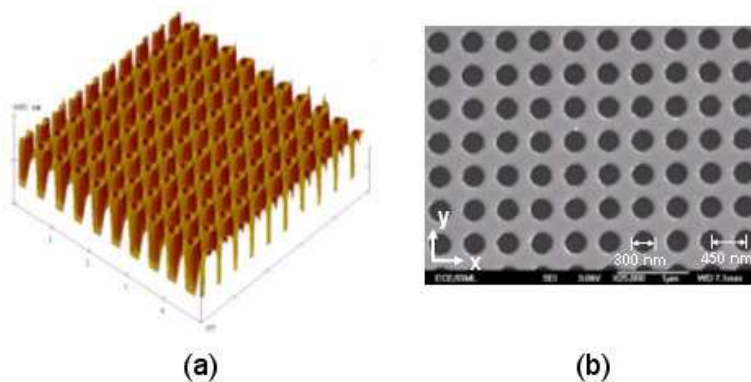


Fig. 4. (a) AFM image of the DUV resist profile for the fabrication of antidot arrays. (b) Scanning electron micrograph of 25-nm-thick $\text{Ni}_{80}\text{Fe}_{20}$ antidot arrays.

of Cr (10 nm)/Au (300 nm). For MR measurements, a dc current of 1 mA was passed along the x -direction, and the resistance was recorded automatically using a four-point probe technique as the in-plane magnetic field was swept at a constant rate. The devices were mounted on an automatic rotary stage that allows for the easy rotation of the devices in the magnetic field. Magnetic hysteresis loops and the magnetic anisotropy distribution in the antidot arrays were obtained using VSM at room temperature.

4 Transport Properties in Antidot Mesostructures

In this section, MR measurements will be used to study the detailed magnetization reversal process of the 25-nm-thick $\text{Ni}_{80}\text{Fe}_{20}$ antidot arrays. We have investigated the effect of current density distribution in the antidot arrays and showed that the MR technique is a powerful and sensitive technique in mapping the magnetization reversal process in nanoscale antidot arrays [31].

The interpretation of the MR measurements in a single layer ferromagnetic material is derived from the well-known anisotropic MR (AMR) effect, which states that the resistance of the ferromagnetic material can be described as

$$R_{(H)} = R_0 + \Delta R \cos^2 \theta, \quad (4)$$

where θ is the angle between the current density and magnetization, R is the film resistance, and $\Delta R = R_{||} - R_{\perp}$ represents the AMR effect.

Since the AMR output depends on two physical terms, the current density and magnetization, it is important to first establish the current density distribution in our antidot structure in order to understand the varying magnetization component. Strictly speaking, the two terms are interdependent. However, due to the small change in AMR percentage (2.5% for a typical thin film), the correlation between the two could be ignored most of the time. Shown in Fig. 5 is the finite element simulation using ANSYS software [32] for the current density distribution without taking into account the galvanomagnetic effect in the circular hole arrays. The arrows signify the direction of current flow at each location, and

the length of the arrow together with the color code indicates the magnitude of the current density. We observed that the current is unidirectional flowing along the x -direction in the hole arrays. It was also noticed that the current density is not uniform but rather periodically modulated by the presence of the antidots. Nearer to the geometrical boundaries of the antidots, the current tends to follow the circumferences of the holes. Deviation from the main current direction and a decrease in current density magnitude are observed as the current density penetrates into the region between the adjacent holes in the same row.

Having established the current distribution in the structure, the MR response could be explained as a measure of the preference of the local spins along the current density direction. We performed the longitudinal MR (LMR) measurements (corresponding to fields applied along the sense current direction (x -direction)) and transverse MR (TMR) measurements (corresponding to fields applied perpendicular to the sense current direction (y -direction)) for the antidot structures. Shown in Fig. 6(a) is the normalized LMR curve of 25-nm-thick $\text{Ni}_{80}\text{Fe}_{20}$ antidot arrays. The gray dots represent the loop with the field sweeping from the negative saturation field to the positive field. The dark dots are the results for the reverse field sweep. We will only examine the loop marked by dark dots, as the two loops are essentially symmetric in nature. Shown as insets in Fig. 6(a) are sketches of the spin states of a unit cell at different field strengths, which is inferred from the MR curve with simple magnetostatics. At a first glance, the MR curve shows two distinct minima, with a series of bends signifying the switching process occurring in the arrays.

At high field, all the spins in the antidot structure are primarily aligned along the field direction, as shown in the schematic illustration A in Fig. 6(a). With the initial reduction of field, a slight linear increase in resistance is observed indicating that the local spins are more aligned with the current density. This is because the current density is not exactly aligned with the magnetization at saturation due to the geometrical confinement

introduced by the holes, as shown in Fig. 5. At a slightly lower field, the spins close to the holes start to align along the edges of the holes to

reduce the associated magnetostatic energy, as illustrated by spin state B in Fig. 6(a). Thus, the average angle between the current density and

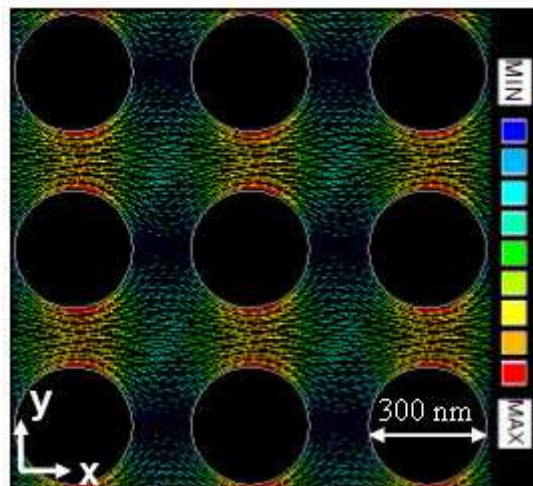


Fig. 5. Finite element current density simulation for the circular antidot arrays. The length of the arrow together with the color code indicates the magnitude of the current density.

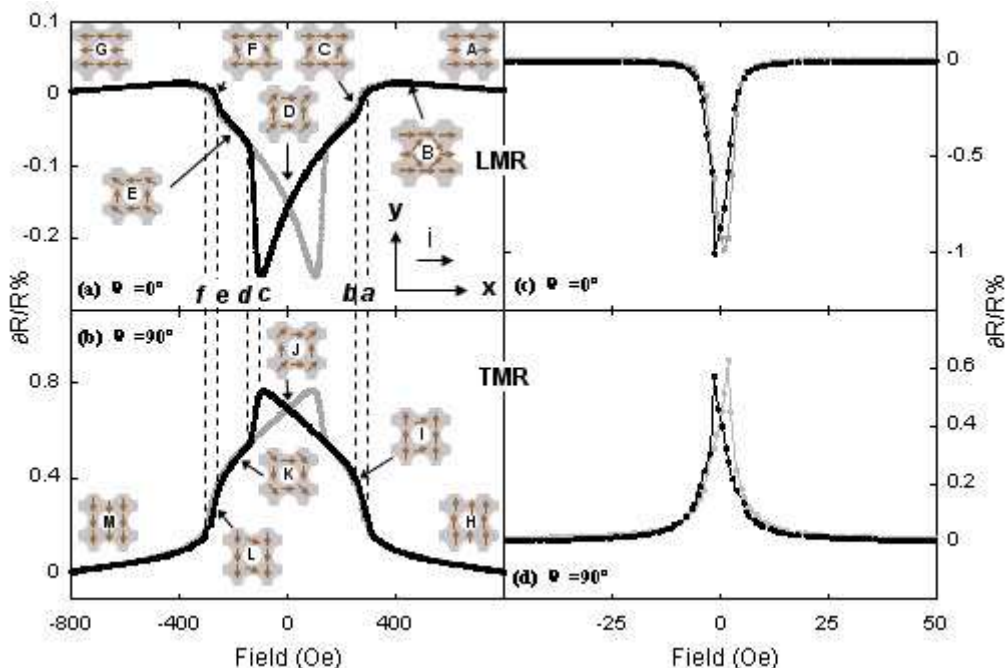


Fig. 6. Normalized (a) LMR curve and (b) TMR curve for the 25-nm-thick $\text{Ni}_{80}\text{Fe}_{20}$ antidot arrays. Shown as insets are the schematic illustrations of the spin states at different field values. The dashed lines indicate the positions where deflections in the MR curve occur. The corresponding MR curves for the 25-nm-thick $\text{Ni}_{80}\text{Fe}_{20}$ continuous films are shown in (c) and (d), respectively.

local spins is reduced, resulting in a higher resistance.

When the field is reduced further, a decrease in resistance is observed followed by a kink at a field of 300 Oe as marked by position *a* in Fig. 6(a). This could be attributed to the continuous rotation of the spins as shown in B resulting in a deviation of the spins from the local current density, which causes this initial decrease in resistance. Starting from position *a*, due to the high shape anisotropy, the local spins to the left and right of the holes start to rotate along the *y*-direction, as illustrated by the inset C. The increase in misalignment of the current density and magnetization in these areas could be responsible for the faster decrease in resistance. The decrease in resistance becomes more gradual again at a field of 238 Oe, as shown at position *b*, indicating the completion of the previous spin rotation process. As the field is reduced to zero, the resistance is further reduced due to the spins at the corners to the holes rotating close to 45° to the *x*-direction, causing a larger angle between the current density and magnetization, as shown in D. This configuration minimizes magnetostatic energy and the net charges around the holes.

As the field changes sign, and increases in magnitude, the resistance decreases continuously. At this field range, due to the strong shape anisotropy imposed by the holes, the reverse domain could not be formed in the arrays initially, and the resistance decrease may still be attributed to the continual rotation of the diagonal spins. At a field of 105 Oe (position *c*), the irreversible switching to reverse magnetization state occurs, as signified by the sudden jump in the curve. The increase in resistance soon becomes gradual after position *d*, as the spins at the corner of the holes start to become pinned along the negative *x*-axis, attaining a spin configuration shown in the spin state E. The completion of this process changes the deflection of the curve at a field of

220 Oe, as shown by position *e*. Further increase in reverse field magnitude causes the spins at the left and right side of the holes to rotate to the field direction as depicted in the spin state F, and the kink at position *f* shows that this process is over.

A similar linear decrease with field is observed again, as the field approaches the reverse saturation field.

Figure 6(b) is the corresponding TMR curve, where the in-plane field is applied perpendicular to the sense current ($\theta = 90^\circ$). The curve consists of a near-parabolic trace with extensive tails at high field and two distinctive peaks at low field. At saturation, the magnetization is perpendicular to the current, resulting in a low resistance, as shown in the spin state H. As the external field is reduced, at first the magnetization above and below the holes starts to rotate along the current direction causing an overall increase in resistance, as shown in the spin state I. The rotation of the spins diagonal to the holes, as shown in the spin state J, contribute to the increase in the resistance value until at a reverse field irreversible switching in magnetization occurs and reaches spin state K. As the field increases in the reverse direction, the spins diagonal to the hole are pinned along the field, leading to a further decrease in resistance, as shown by state L. This decrease starts to become stable after the spins below and above the holes are perpendicular to the current in the opposite direction, as sketched in the spin state M. From the above description, it is not difficult to see that the magnetization reversal process in the TMR measurement is very similar to that of LMR. Owing to the symmetry of the square antidot lattice, the TMR measurement here is equivalent to the setup whereby the field orientation is fixed as in the LMR measurement and then the current direction is rotated by 90°. Hence, the two curves in Fig. 6(a) and (b) are actually describing the same magnetization reversal process in the antidot structure. This is evident from the spin state illustration as well as the switching positions marked by the dotted lines in the figures.

Compared with the antidot arrays, the 25-nm-thick Ni₈₀Fe₂₀ continuous film without the holes deposited under the same condition shows completely different MR characteristics, as the reversal process in the continuous film is mediated by the domain wall movement. As shown in Fig. 6(c) and (d), the continuous film displays a typical negative MR ratio for LMR and positive MR ratio

for TMR measurement with a low saturation field of about 10 Oe and switching field at only 1.2 Oe, which are much lower than those of the antidot arrays.

5 Lattice Geometry Dependence of Magnetic Anisotropy

This section will focus on the effect of antidot lattice geometry on magnetic anisotropy of the thin film, which is explored by fabricating ferromagnetic antidot arrays with square, honeycomb, and rhomboid lattice arrangements. A systematic study on the field orientation dependence of the remanence magnetization as well as micromagnetic spin states has been carried out [33]. The shape of the antidots is chosen to be circular, so that the hole itself does not contribute to the anisotropy of the antidot structure. Shown in Fig. 7(a) and (c) are the SEM images for the resist dots forming square, honeycomb, and rhomboid arrays, respectively. $\text{Ni}_{80}\text{Fe}_{20}$ film of thickness 30 nm was then deposited using e-beam evaporation. The final structure consists of $\text{Ni}_{80}\text{Fe}_{20}$ arrays of antidots of diameter 250 nm and the center-to-center spacing between nearest holes is 400 nm, as shown in Fig. 7(d)–(f).

The magnetic anisotropy distribution of the antidot arrays was measured using a vibrating sample magnetometer. To characterize the magnetic anisotropy, we have measured the remanence magnetization as a function of the orientation of the applied field. This was performed by first saturating the sample at 2 kOe in a given in-plane direction, then reducing the field to zero before measuring the remanent magnetization (M_r). This process was repeated at an incremented field orientation.

Figure 8(a) shows the normalized remanent magnetization (squareness M_r/M_s) with the corresponding mapping of the easy and hard axes for the unpatterned 30-nm-thick $\text{Ni}_{80}\text{Fe}_{20}$ film, which was deposited at the same time with the antidot structures, also acting as the control experiment. The blue dots represent the experimental data and the continuous red line is the fitted curve. From the figure, we observed that the unpatterned film

exhibits a weak uniaxial anisotropy as expected with squareness ranging from 0.62 to 0.71, due to the polycrystalline nature of the film and the absence of field-induced anisotropy.

With the introduction of square lattice antidots, the 30 nm $\text{Ni}_{80}\text{Fe}_{20}$ film shows a well-defined fourfold (bi-axial) anisotropy with the HAs along the edges of the square unit cell, and the EAs along the diagonal direction, as shown in Fig. 8(b). The shape of the curve is fitted well by an offset $j\sin 2\theta_j$ function varying between 0.55 and 0.8, as depicted by the continuous line. The observed periodicity of the anisotropy is because the sample is geometrically equivalent as the array is rotated for every 90° .

By changing the antidot lattice geometry from square to honeycomb, we observed that the magnetic anisotropy changes from a four- to sixfold symmetry, respectively. The hard and easy axes alternate at every 30° for the honeycomb geometry, as shown in Fig. 8(c). Similar to the case of square arrays, the HAs for the honeycomb geometry remain parallel to the edges of the hexagonal unit cell. The anisotropy distribution for the honeycomb lattice generally follows a $j\sin 3\theta_j$ variation, and the squareness varies between 0.71 and 0.81.

The space arrangement of the rhomboid lattice is closely related to the honeycomb lattice, as the unit cell can be taken as a hexagon cell of the honeycomb lattice embedded with an additional hole in the center. The introduction of this extra hole, however, markedly changes the anisotropy distribution of the arrays. As can be seen from Fig. 8(d), although a sixfold magnetic anisotropy and similar squareness is observed, there is a 30° phase shift in the curve as compared with the honeycomb lattice in Fig. 8(c), indicating a reverse of the EA and HA orientations.

To explain the magnetic anisotropy behavior obtained in Fig. 8, an understanding of the distribution of the microscopic spin orientations in the samples is needed, since the net magnetic moment along the applied field leads to the observed remanent magnetization. This was achieved by performing micromagnetic simulations for the remanent spin states using OOMMF

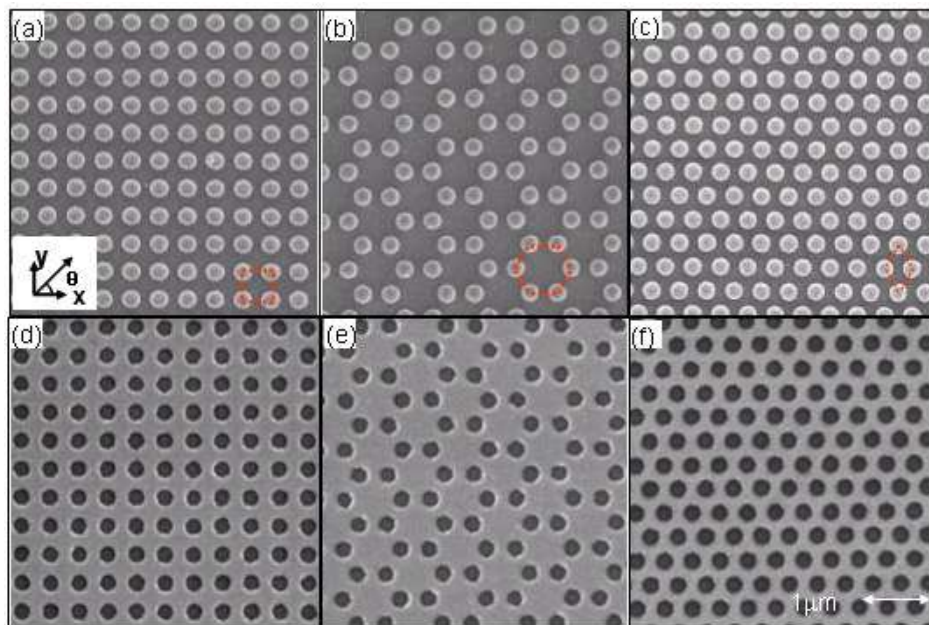


Fig. 7. SEM images of resist patterns for (a) square, (b) honeycomb, and (c) rhomboid lattice geometry. The corresponding SEM images of 30-nm-thick $\text{Ni}_{80}\text{Fe}_{20}$ antidot arrays after the liftoff process are shown in (d)–(f), respectively.

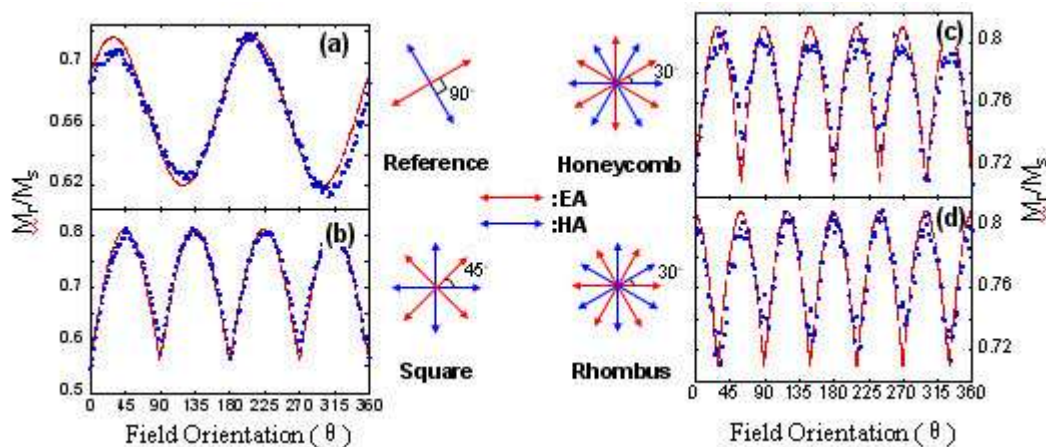


Fig. 8. The normalized remanent magnetization (squareness M_r/M_s) as a function of field orientation θ for (a) reference continuous film, (b) square lattice, (c) honeycomb lattice, and (d) rhomboid lattice 30-nm-thick $\text{Ni}_{80}\text{Fe}_{20}$ antidot arrays. The dotted traces are experimental data, and the continuous lines were obtained from curve-fitting. Besides the curves are the easy axis (EA) and hard axis (HA) distribution of the respective lattice geometry.

software package [34]. The magnetic parameters used for simulations are saturation magnetization $M_s = 860 \text{ kA/m}$, exchange constant $A = 13 \times 10^{-12} \text{ J m}^{-1}$, and anisotropy constant $K_u = 0$. A cell size of 10 nm was used in computation. The convergence criterion was a misalignment between magnetization and effective field

($j_m - h_j$) lower than 10^{-5} in every cell. We simulated spin states of the $\text{Ni}_{80}\text{Fe}_{20}$ antidot structure with the identical dimensions as those shown in Fig. 7 for 30 nm film thickness. The remanent states were obtained by capturing the spin states of the antidot structures after removal of a saturation field along one of the easy axes of the

structures, namely at $\theta = 45^\circ, 30^\circ$, and 0° for the three arrays, as shown in Fig. 9(a), (c), and (e). The simplified illustrations for the magnetic domains inside a square and hexagonal unit cell are next to the captured spin states, as shown in Fig. 9(b) and (d). For the rhomboid antidot lattice, the domain sketch of a seven-hole hexagonal cell in Fig. 9(f) is shown to compare with the honeycomb lattice.

For the square lattice, we observed a remanent state with periodic microscopic domains in the vicinity of the holes, which is depicted in Fig. 9(a). The spin configuration is apparently different from the blade domains usually nucleated around the isolated holes to reduce the surface magnetic charges, as illustrated in the inset of Fig. 9(b). This shows that the remanent spin state of the antidot arrays is not only a result of the minimization of the magnetostatic energy of each hole itself, but also the magnetostatic interaction between the neighboring holes. From the sketch, the magnetic material in the unit cell can be roughly divided into five domains. The domains with spins pointing along the x - and y -directions are formed to decrease the high demagnetizing

energy due to the close edges of the nearest neighboring holes. The 45° domain bisecting the previous two types of domains is nucleated to reduce the associated magnetostatic energy.

The remanent state of the honeycomb lattice captured from simulation is shown in Fig. 9(c). The hexagonal cell could be roughly divided into nine microscopic domains, as shown in Fig. 9(d). One common feature of the spin states between the hexagonal and square lattices is that the material between the nearest neighboring holes is still highly confined by the edges of holes, so that the spins in those areas are always aligned perpendicular to the edges of the unit cell. Because of the symmetry, the vector sum of the magnetization in these areas is at about 30° . In the center of the lattice, we observed a parallelogram shaped domain pointing at slightly above 30° , flanked by two triangular shaped domains with magnetization along the positive x -direction. After analyzing the overall magnetization of the unit cell, the normalized net remanent magnetization is about 0.85 at 29.4° , which is consistent with the experimental result.

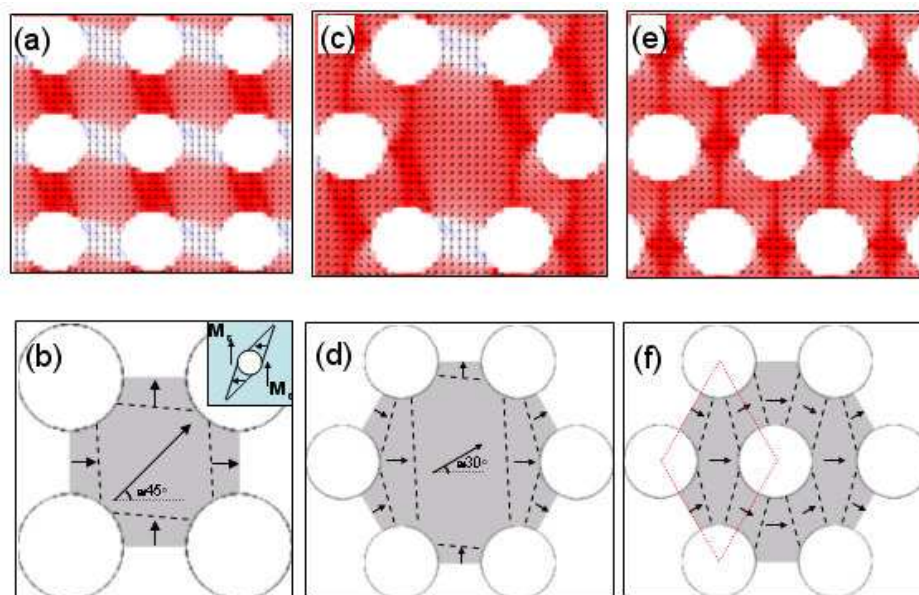


Fig. 9. The remanent spin states in a unit cell captured from the micromagnetic simulation and the simplified domain distributions are shown for (a), (b) the square lattice, (c), (d) the honeycomb lattice, and (e), (f) the rhomboid lattice 30-nm-thick $\text{Ni}_{80}\text{Fe}_{20}$ antidot arrays. Note: Drawings are not to proportion for the clarity of presentation.

With the introduction of an additional hole to the hexagonal unit cell shown in Fig. 9(c), a completely different remanent spin state in Fig. 9(e) is observed. The 30° and 90° domains around the central axis of the honeycomb unit cell have been replaced by the 0° and 30° domains, which explains the striking change in the distribution of easy and hard axes in Fig. 8(c) and (d). From the sketch in Fig. 9(f), it can be easily identified that the average spin orientation is along the x -direction, which makes 0° the preferred direction for magnetization. The magnetic domains in the rhomboid lattice arrays can generally be divided into two groups. One group are those having an angle of 30° to the x -axis. The formation of these domains is a result from the shape anisotropy imposed by the two nearest neighboring holes. The other group of domains are pinned along the x -direction. They occur in the central region among the nearest four holes forming a rhomboid cell, e.g. the area enclosed by the dotted lines. It is interesting to note that despite the high demagnetizing field at the hole edges, the remanent spins between the two nearest holes in the same row remain at this unfavorable high magnetostatic energy configuration. This is because the energy gain from this configuration reduces the surrounding exchange energy across the domain walls significantly.

The remanent spin states shown in Fig. 9 are not limited to the EA field alone, similar spin configurations were also obtained for fields applied along other field orientations. This implies that those spin states are the only possible configurations at remanence. The remanence magnetization measured at certain field orientations are therefore a projection of the net magnetization along the nearest EA, which confirms the validity of the curve fit for the experimental data, and explains the reduced amplitude of squareness for highly symmetric arrays shown in Fig. 8.

6 Multilayer Antidot Arrays

While a lot of research has been focused on single layer ferromagnetic antidot nanostructures,

today very little data are available on their multilayer counterparts [35, 36]. However, the large surface area present at the edges of the antidot arrays could induce edge charges, which provide us with a unique model to study the magnetostatic interaction between the magnetic layers. The spin-dependent transport mechanism in the multilayer structure is also dramatically different from the single layer structure, as the magnetoresistance signals may be strongly influenced by the relative spin orientation between the adjacent ferromagnetic layers, which gives rise to giant MR [37] or tunneling MR effect [38]. For the GMR effect to occur in multilayer systems, usually two ferromagnetic (FM) layers separated by a nonmagnetic conducting spacer layer are needed. The resistivity is a maximum when the directions of the magnetization in the two FM layers are antiparallel and a minimum when they are parallel. The phenomenological dependence of the resistivity on the relative orientation (α) of the magnetization in the two FM layers can be written as

$$\rho_{G(\alpha)} = \rho_{G//} + \Delta\rho_G \cos \alpha, \quad (5)$$

where $\rho_{G//}$ is the resistivity for ferromagnetic layers with parallel magnetization, and $\Delta\rho_G$ is the difference in resistivity between the antiparallel and parallel magnetization cases.

In this section, a systematic investigation has been conducted on the magnetic and transport properties of pseudo-spin-valve antidot structures consisting of Co (30 nm)/Cu (t_{Cu} nm)/Ni₈₀Fe₂₀ (30 nm) [39]. The antidot arrays are of square lattice geometry and the lateral dimensions are the same as those shown in Fig. 7(d). The spacer thickness, t_{Cu} , was varied from 2 to 30 nm, as illustrated in Fig. 10.

Shown in Fig. 11(a) are representative hysteresis loops for fields applied along the easy axis of the square lattice antidot arrays as a function of Cu spacer layer thickness. The loops are strongly dependent on the thickness range due to the different coupling mechanisms that mediate the magnetization reversal processes. For $t_{Cu} = 2$ nm, the two FM layers switch nearly in unison with a sharp transition, having a similar

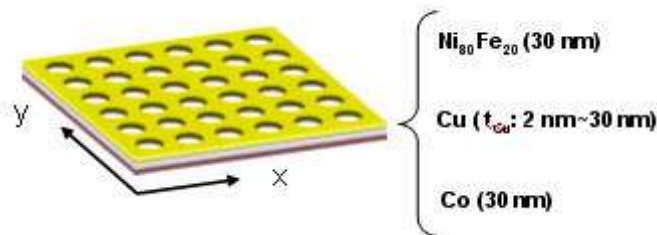


Fig. 10. The schematic illustration for the composition of multilayer antidot arrays.

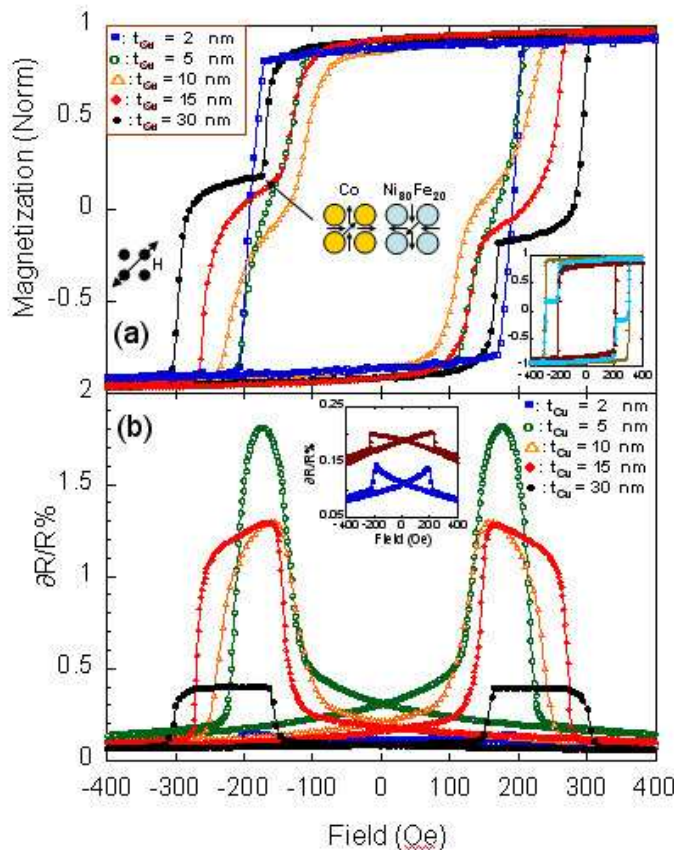


Fig. 11. (a) Representative magnetic hysteresis loops of Co (30 nm)/Cu (t_{Cu} nm)/Ni₈₀Fe₂₀ (30 nm) antidot nanostructures as a function of Cu spacer layer thickness (t_{Cu}) for fields applied along the easy axis. The magnetic hysteresis loops from single layer Ni₈₀Fe₂₀ (⊙) and Co(+) antidot nanostructures, and the interpolated loop (θ) assuming no coupling between the two FM layers are shown as inset. (b) The corresponding normalized MR curves as a function of t_{Cu} for fields applied along the easy axis of the arrays.

shape to the response from a single layer Co or Ni₈₀Fe₂₀ antidot film shown in the inset. This may be attributed to the strong ferromagnetic exchange coupling through the Cu spacer layer. As t_{Cu} increases to 5 nm, the strength of exchange coupling becomes weaker, and the antidot film

switches to the reverse magnetization through a two-step switching, which is initiated by the switching of the soft layer (Ni₈₀Fe₂₀) followed by the hard layer (Co). We also observed a dramatic decrease in the onset of the switching field of the Ni₈₀Fe₂₀ layer from 170 Oe ($t_{Cu} = 2$ nm)

to 108 Oe ($t_{Cu} = 5$ nm). This could be attributed to the influence from the magnetostatic coupling between the two FM layers due to the stray field from the edge of the holes, as the interlayer magnetostatic interaction favors an antiferromagnetic order. For $t_{Cu} = 10$ nm, the antidot film is effectively exchange decoupled due to the short-range nature of the exchange interaction, and the onset switching field of the $Ni_{80}Fe_{20}$ layer is reduced again to 62 Oe due to magnetostatic coupling. Further increase in t_{Cu} to 15 nm weakens the magnetostatic coupling, and causes an increase of the onset switching field to 82 Oe. For $t_{Cu} = 30$ nm, the reversal of the two layers are almost independent as evident by the two sharp transitions separated by a relatively stable plateau, which corresponds to an antiparallel spin alignment between the FM layers, as illustrated by the spin states of both the Co and $Ni_{80}Fe_{20}$ layers. At this thickness, the shape of the hysteresis loop resembles that of the interpolated loop shown in the inset, where no coupling effect is assumed.

To understand the transport mechanism in the multilayer square lattice antidot nanostructures, MR measurements were performed. Shown in Fig. 11(b) are the representative MR curves for fields applied along the easy axis as a function of Cu spacer layer thickness corresponding to the M-H loops shown in Fig. 11(a). For $t_{Cu} = 2$ nm, the synchronized reversal of the two FM layers leads to a typical anisotropic MR (AMR) response with a maximum MR ratio of about 0.14%. The shape of the curve is similar to the single layer 30-nm-thick $Ni_{80}Fe_{20}$ antidot film, as reproduced in the inset of the figure. For $t_{Cu} > 2$ nm, however, the MR response is governed by the giant magnetoresistance (GMR) effect at low field, and the GMR ratio is significantly dependent on the spacer layer thickness. The highest MR ratio of 1.8% occurs for $t_{Cu} = 5$ nm and it gradually decreases for larger t_{Cu} . One of the reasons for the decrease is the current shunting effect by the Cu layer. In addition, the variation in transmission without scattering for polarized electrons through the spacer layer drops with increasing t_{Cu} . Another noticeable difference among the curves is the sharpness

of the peaks, which signifies the stiffness of holding antiparallel spin alignment during the magnetization reversal processes. As the spacer layer becomes thicker, the peaks become wider and flatter, which can be correlated to the kinks in the magnetic hysteresis loops in Fig. 11(a).

We also performed the longitudinal MR (LMR) measurements (corresponding to fields applied along the x -direction) and transverse MR (TMR) measurements (corresponding to fields applied along the y -direction) for the different trilayer structures. Shown in Fig. 12 are the representative LMR and TMR curves as a function of spacer layer thickness. As can be seen, the MR curves are characterized by the interplay of the AMR and GMR effect resulting in an interesting evolution of transport properties.

For $t_{Cu} = 2$ nm, we observed two distinct minima in the LMR curve at low field arising from the AMR effect, as depicted in Fig. 12(a). For $t_{Cu} = 5$ nm, however, the GMR effect reverses the sign of LMR curve completely, giving rise to a high resistance at low field, as shown in Fig. 12(b). The AMR component, though small in magnitude, still leaves its traces in the form of a small valley before the onset of the peaks. As t_{Cu} is increased further, the valley becomes deeper and starts to shift further to the reverse field, which reveals an increasing AMR effect in the LMR curves.

The TMR curves can also be explained using a combination of AMR and GMR effects. For $t_{Cu} = 2$ nm, as expected, the TMR curve is characterized by a bell-like shaped curve with two peaks at low field due to the AMR effect. For $t_{Cu} = 5$ nm in (b), in contrast to the corresponding LMR curve, which exhibits only two peaks, the TMR curve features multiple peaks. By tracing the curve as the magnetic field is swept from negative saturation to the positive (black dots), we observed three peaks (P_1 to P_3) at fields of -440, 105, and 526 Oe, respectively. The occurrence of P_1 and P_3 may be attributed to the different spin orientations of the two FM layers in response to the high demagnetizing field at hole edges, as illustrated in a simplified spin state configuration in Fig. 12(b). Peak P_2 results from the GMR effect due to the reverse magnetization in the

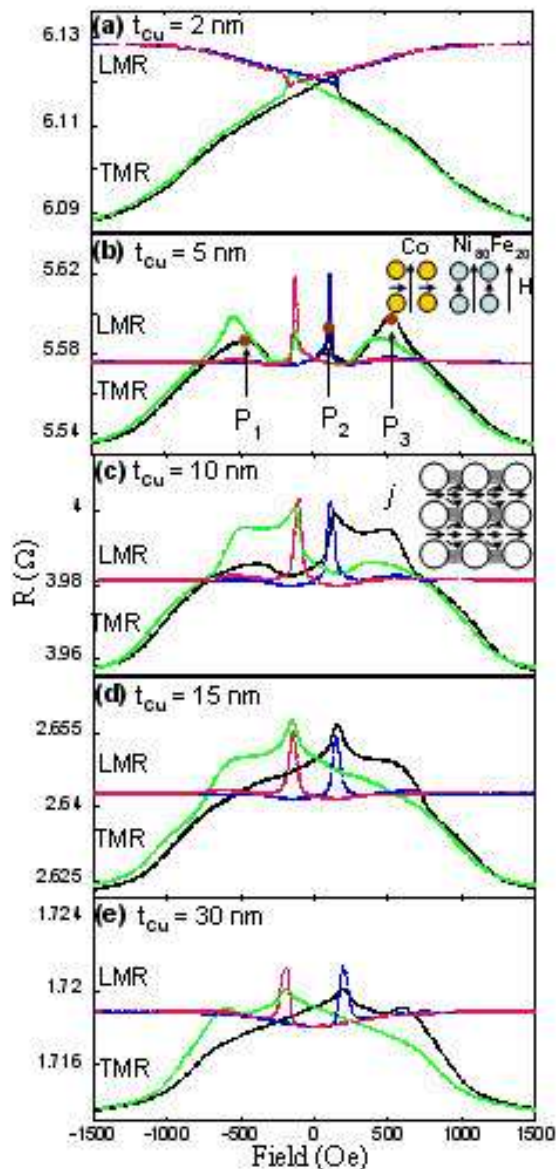


Fig. 12. LMR and TMR curves of the Co (30 nm)/Cu (t_{Cu} nm)/Ni₈₀Fe₂₀ (30 nm) antidot arrays as a function of t_{Cu} . The red and blue dots represent the backward and forward sweeping loops of the LMR curves, while the green and black dots similarly represent the respective loops of the TMR curves.

Ni₈₀Fe₂₀ layer, which also causes a peak at the same field in the corresponding LMR curve. We, however, observed no significant change in resistance around the fields at P_1 and only a slight bump at P_3 in the LMR curve. A similar discrepancy is also found for larger spacer thickness shown in Fig. 12(c)–(e). This appears to be strange at first glance because the magnetization reversal

processes in the LMR and TMR measurements are virtually equivalent due to the array symmetry and the GMR effect is independent of the current direction. To understand this discrepancy, we have considered the effect of inhomogeneous current density distribution in the antidot arrays, as illustrated in the inset of Fig. 12(c). Since MR is only sensitive to magnetization in the current

path, the spin configuration (inset of Fig. 12(b)) responsible for P_1 and P_3 in the TMR curves leads to a much reduced GMR effect in the LMR measurement.

The interplay between AMR and GMR also has great impact on the shape of the TMR curves as the spacer layer thickness is varied. With increasing t_{Cu} , the amplitude of P_1 and P_3 generally decreases, and for $t_{Cu} = 30$ nm, the trace of P_1 is not visible as we observed a monotonic increase in resistance before the external field changes sign. In contrast, P_2 has an increased magnitude with t_{Cu} , and remains as the global maxima in the curves.

The MR responses from the continuous trilayer films deposited at the same time as the respective antidot arrays presented in Fig. 12 were also measured. In contrast to the antidot arrays, we observed that for $t_{Cu} = 15$ nm, the LMR resistance of the continuous film is dominated by AMR effect, and the onset of positive GMR peaks was only noticed for $t_{Cu} = 30$ nm as shown in Fig. 13. This observation is very interesting as it reveals that GMR effect could be induced by the introduction of hole defects into the continuous film. The origin of this induced GMR may be attributed to the high differential coercivity

between the Co and $Ni_{80}Fe_{20}$ antidot FM layers. In addition, the strong magnetostatic coupling between the two FM layers due to the magnetic charges in the vicinity of the holes helps to stabilize the antiparallel relative spin alignment, and thus enhance the GMR effect.

7 Conclusion

In summary, we have shown that the magnetic and transport properties of the ferromagnetic film could be strongly modified by the presence of engineered defects. We studied the transport properties of nanoscale $Ni_{80}Fe_{20}$ antidot arrays with square lattice geometry, revealing the local spin state evolution around the hole. Compared with the continuous film, a dramatic increase in switching field of the antidot structures due to the local modification of the spin configurations was observed.

We have shown that by tailoring the antidot lattice geometry, systematic modification of the magnetic anisotropy distribution in the ferromagnetic films can be achieved. For an antidot array with a square lattice, a fourfold magnetic anisotropy with alternating hard and easy axis at every 45° was observed. The honeycomb and rhomboid antidot lattice both show a sixfold

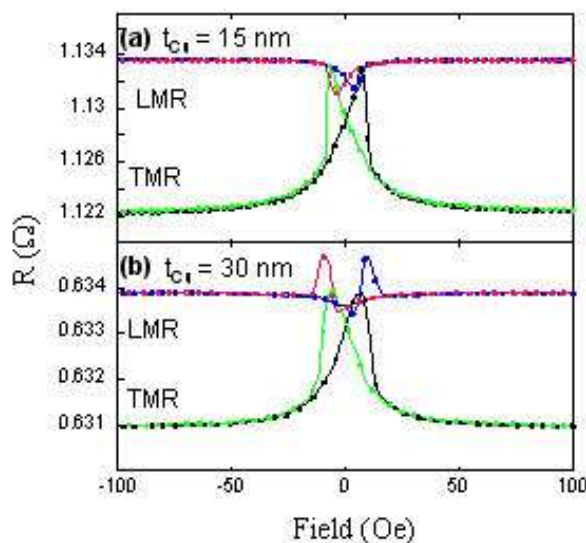


Fig. 13. LMR and TMR curves of the Co (30 nm)/Cu (t_{Cu} nm)/ $Ni_{80}Fe_{20}$ (30 nm) continuous reference film for $t_{Cu} =$ (a) 15 nm and (b) 30 nm, respectively.

anisotropy conforming well to the symmetry of their respective lattices.

We have also investigated the magnetic and transport properties of multilayer antidot nanostructures. The magnetization reversal processes were observed to be markedly dependent on spacer layer thickness. The transport properties of the antidot arrays typically show a superposition of anisotropic and giant magnetoresistance effects, and the relative magnitude of the two effects is strongly sensitive to the spacer layer thickness. The corresponding continuous multilayer films, however, exhibit a different MR response, as the onset of the giant magnetoresistance effect was only observed at much higher spacer layer thickness.

References

- [1] C. Shearwood, S. J. Blundell, M. J. Baird, J. A. C. Bland, M. Gester, H. Ahmed, and H. P. Hughes, *J. Appl. Phys.* **75**, 5249 (1994).
- [2] S. Goolaup, N. Singh, A. O. Adeyeye, V. Ng, and M. B. A. Jalil, *Eur. Phys. J. B* **44**, 259 (2005).
- [3] R. P. Cowburn, *J. Phys. D: Appl. Phys.* **33**, R1 (2000).
- [4] J. K. Ha, R. Hertel, and J. Kirschner, *Phys. Rev. B* **67**, 224432 (2003).
- [5] S. Goolaup, N. Singh, and A. O. Adeyeye, *J. Phys. D: Appl. Phys.* **38**, 2749 (2005).
- [6] M. Kläui, J. Rothman, L. Lopez-Diaz, C. A. F. Vaz, J. A. C. Bland, and Z. Cui, *Appl. Phys. Lett.* **78**, 3268 (2001).
- [7] J. Wang, A. O. Adeyeye, and N. Singh, *Appl. Phys. Lett.* **87**, 262508 (2005).
- [8] C. A. Ross, *Annu. Rev. Mater. Res.* **31**, 203 (2001).
- [9] A. Moser, K. Takano, D. T. Margulies, M. Albrecht, Y. Sonobe, Y. Ikeda, S. Sun, and E. E. Fullerton, *J. Phys. D: Appl. Phys.* **35**, R157 (2002).
- [10] J. M. Slaughter, R. W. Dave, M. DeHerrera, M. Durlam, B. N. Engel, J. Janesky, N. D. Rizzo, and S. Tehrani, *J. Supercond.* **15**, 19 (2002).
- [11] R. P. Cowburn and M. E. Welland, *Science* **287**, 1466 (2000).
- [12] D. A. Allwood, G. Xiong, M. D. Cooke, C. C. Faulkner, D. Atkinson, N. Vernier, and R. P. Cowburn, *Science* **296**, 2003 (2002).
- [13] G. Csaba, W. Porod, and Á. Csurgay, *Int. J. Circ. Theor. Appl.* **31**, 67 (2003).
- [14] A. Imre, G. Csaba, L. Ji, A. Orlov, G. H. Bernstein, and W. Porod, *Science* **311**, 205 (2006).
- [15] R. P. Cowburn, A. O. Adeyeye, and J. A. C. Bland, *J. Magn. Mater.* **173**, 193 (1997).
- [16] W. Y. Lee, H. T. Leung, W. Zhang, Y. B. Xu, A. Hirohata, C. C. Yao, B.-Ch. Choi, D. B. Hasko, and J. A. C. Bland, *IEEE. Trans. Magn.* **35**, 3475 (1999).
- [17] A. O. Adeyeye, J. A. C. Bland, and C. Daboo, *Appl. Phys. Lett.* **70**, 3164 (1997).
- [18] U. Welp, V. K. Vlasko-Vlasov, G. W. Crabtree, C. Thompson, V. Metlushko, and B. Ilic, *Appl. Phys. Lett.* **79**, 1315 (2001).
- [19] C. T. Yu, H. Jiang, L. Shen, P. J. Flanders, and G. J. Mankey, *J. Appl. Phys.* **87**, 6322 (2000).
- [20] I. Guedes, N. J. Zaluzec, M. Grimsditch, V. Metlushko, P. Vavassori, B. Ilic, P. Neuzil, and R. Kumar, *Phys. Rev. B* **62**, 11719 (2000).
- [21] A. Yu. Toporov, R. M. Langford, and A. K. Petford-Long, *Appl. Phys. Lett.* **77**, 3063 (2000).
- [22] Robert C. O'Handley, *Modern Magnetic Materials: Principles and Applications*, New York: Wiley (2000), p. 328.
- [23] H. Barkhausen, *Phys. Z.* **29**, 401 (1919).
- [24] M. Kersten, *Phys. Z.* **44**, 63 (1943).
- [25] L. Néel, *Cahiers de Phys.* **25**, 21 (1944).
- [26] H. J. Williams, *Phys. Rev.* **71**, 646 (1947).
- [27] W. D. Nix and R. A. Huggins, *Phys. Rev.*, **A135**, 401 (1964).
- [28] J. C. Brice, *Brit. J. Appl. Phys.* **16**, 1523 (1965).
- [29] A. Butera, J. L. Weston, and J. A. Barnard, *IEEE Trans. Magn.* **34**, 1024 (1998).
- [30] N. Singh, S. Goolaup, and A. O. Adeyeye, *Nanotechnology* **15**, 1539 (2004).
- [31] C. C. Wang, A. O. Adeyeye, N. Singh, Y. S. Huang, and Y. H. Wu, *Phys. Rev. B* **72**, 174426 (2005).
- [32] ANSYS Release No. 5.7, Swanson Analysis Systems, Inc., Houston, PA (2002).
- [33] C. C. Wang, A. O. Adeyeye, and N. Singh, newline *Nanotechnology* **17**, 1629 (2006).
- [34] M. J. Donahue and D. G. Porter, <http://math.nist.gov/oommf>
- [35] F. J. Castaño, K. Nielsch, C. A. Ross, J. W. A. Robinson, and R. Krishnan, *Appl. Phys. Lett.* **85**, 2872 (2004).
- [36] T. L. Hylton, M. A. Parker, K. R. Coffey, J. K. Howard, R. Fontana, and C. Tsang, *Appl. Phys. Lett.* **67**, 1154 (1995).
- [37] E. Tsymlal and D. G. Pettifor, *Solid State Phys.* **56**, 113 (2001).
- [38] M. Julliere, *Phys. Lett. A* **54**, 225 (1975).
- [39] C. C. Wang, A. O. Adeyeye, and N. Singh, *Appl. Phys. Lett.* **88**, 222506 (2006).

Forthcoming Conferences

SSI-16

1-6 July 2007, Shanghai, China

The 16th International Conference on Solid State Ionics, dealing with the fundamentals, innovations, and applications in the field of ion transport in solids will be held in Shanghai, China. The conference will have several plenary presentations, keynote lectures, and invited talks as well as contributed oral and poster presentations. An exhibition of equipment, products, instrumentation, software, publications, and services will also be held.

For further information, contact: ssi-16@mail.sic.ac.cn; also see: www.SSI-16.net

Materials Today Asia

3-5 September 2007, Beijing, China

This new international conference, organized by Elsevier/Materials Today, will address the latest developments in three novel and exciting areas of Materials Research. Plenary and selected contributed papers will be arranged within three symposia:

Synthesis and Assembly of Nanostructures

Symposium chair:

Yunan Xia *University of Washington, USA*

Functional Materials for Nonvolatile Memories

Symposium chair:

Sang Ho Lim *Korea University, Korea*

The Interface Between Biology and Materials

Symposium chair:

Dan Luo *Cornell University, USA*

Abstracts on the above themes are invited for oral and poster presentations at the conference and should be submitted online at <http://www.materialstodayasia.elsevier.com> by 16 March, 2007.

Website: <http://www.visionresearch-conference.elsevier.com>

17th IKETANI International Symposium

5-7 September 2007, Tokyo, Japan

The 17th IKETANI International Symposium on "Dreams, Creation and Realization of Materials Saving the Humankind" will be held at the University of Tokyo, Japan, during 5-7 September 2007. This symposium is also planned in commemoration of the 80th birthday of Prof. Masao Doyama of Japan.

For more information, contact:

Prof. A. Suzuki, (Suzuki@post.me.ynu.ac.jp) and see the website: www.iketani2007.jks.ynu.ac.jp

IUMRS–ICAM-2007

8–13 October 2007, Bangalore, India

The International Conference on Advanced Materials (ICAM-2007) will consist of at least 24 symposia covering various aspects of Materials Science, Engineering, and Technology consisting of plenary, invited, and public lectures, oral and poster paper presentations. An exhibition of equipment, products, instrumentation, software, publications, and services will also be held.

For further information and correspondence:

Prof. S.B. Krupanidhi (Chair) and Prof. K.T. Jacob (Co-Chair)
IUMRS-ICAM Secretariat, Materials Research Society of India (MRSI)
Indian Institute of Science Campus, Bangalore 560 012, India
E-mail: secretariat@icam2007.com; info@icam2007.com

Contents of the previous issues of 'MRS-S OUTLOOK'

(Vol.1, No.1, July–Sept., 2006)

Editorial

MRS-S Activities: Past, present and future

MRS-S Executive Committee

Message from the Founding President

MRS-S Forthcoming Conference: ICMAT2007

Highlights of the Recent Literature

Materials Education & Research in Singapore

Theme Article: 'Perovskite structure: A Versatile and Perennial Host for Oxide Functional Materials', by G.V. Subba Rao and B.V.R. Chowdari

MRS-S Membership: How to become a Member

Conference Report: ICMAT2005-ICAM 2005

Invitation to MRS-S Members to contribute to 'MRS-S OUTLOOK'

Forthcoming Conferences in the Areas of Materials Science, Engineering and Technology.

(Vol.1, No.2, Oct.–Dec., 2006)

MRS-S Activities: Past, present and future

MRS-S Executive Committee

MRS-S Forthcoming Conference-ICMAT 2007

Report on the 2nd MRS-S National Conference

Singapore-MIT Alliance

Highlights of the Recent Literature

Forthcoming Conferences

Theme Article: 'Drug Eluting Biodegradable Polymers for Biomedical Stent Implants', by Xiong Ying, Wang Xintong, Subbu Venkatraman, Loo Say Chye, Tan Lay Poh and Freddy Boey

Materials Education & research in Singapore

Conference Report: 10th ASSIS Conference held in Sri Lanka

Contents of the First Issue of 'MRS-S OUTLOOK'

Invitation to MRS-S Members to contribute to 'MRS-S OUTLOOK'

(Vol.1, No.3, Jan.-Mar., 2007)

MRS-S Activities: Past, present and future

MRS-S Forthcoming Conference

Highlights of the Recent Literature

Brief write-ups on the following published papers:

'Electrodes with high power and high capacity for rechargeable lithium batteries', K. Kang *et al.*, *Science* **311** 977-980 (2006).

'Sorting carbon nanotubes by electronic structure using density differentiation', M.S. Arnold *et al.*, *Nature Nanotech.* **1** 60-65 (2006).

'Self-regenerating Rh-and Pt-based perovskite catalysts for automotive-emission control', H. Tanaka *et al.*, *Angew. Chem. Int. Ed.* **45** 5998-6002 (2006).

Recent Books in the Area of Materials Science, Engineering and Technology

Announcing the availability of the following books:

'Computational Chemistry of Solid State Materials. A Guide for Materials Scientists, Chemists, Physicists and Others', by Richard Dronskowski, Wiley-VCH, Weinheim, 2005.

'Organic Light-Emitting Devices. Synthesis, Properties and Applications', Edited by Klaus Müllen and Ullrich Scherf, Wiley-VCH, Weinheim 2006.

'The Nanotech Pioneers. Where Are They Taking Us?', by Steven A. Edwards, Wiley-VCH, Weinheim, 2006.

'High Temperature Superconductor Bulk Materials' by Gernot Krabbes, Günter Fuchs, Wolf-Rüdiger Canders, Hardo May and Ryszard Palka, Wiley-VCH, Weinheim 2006.

Theme Article: 'The National University of Singapore Nanoscience and Nanotechnology Initiative (NUSNNI)', by Teik-Cheng Lim, Xian-Ning Xie, Andrew Thye Shen Wee and Seeram Ramakrishna, National University of Singapore (NUS), Singapore. Abstract: This paper highlights some of the nanomaterials-related research work carried out by various Project Investigators under the NUSNNI.

Forthcoming Conferences

Contents of the previous issues of 'MRS-S OUTLOOK'

Invitation to contribute to 'MRS-S OUTLOOK'

Interested readers may write to the Editor (phyvsg@nus.edu.sg) for a reprint, or access the pdf version from the website:www.mrs.org.sg.

INVITATION

MRS-S members are welcome to contribute to 'MRS-S OUTLOOK'

- To suggest topics and prospective author(s) for 'thematic' articles pertaining to the areas of materials science, engineering and technology. These will be of general interest to the students, teachers as well as active researchers. These can be 10–15 pages (A4-size, single spaced) with figures, tables and select references.
- To contribute reports on the recently held conferences and information on the forthcoming conferences.
- To contribute 'Highlights from Recent Literature' in the areas of materials science, engineering and technology. These must pertain to the year 2006 and 2007, and be of general interest to non-specialists, students, teachers as well as active researchers. Each 'Highlight' must not exceed 250–300 words, including reference(s). Contributing author(s) and e-mail address(es) will be included under each 'Highlight'.
- To contribute information about the recent awards and distinctions conferred on the MRS-S members.
- To contribute 'Letters to the Editor'. They may be edited for brevity, clarity and available space, and the author(s) will be informed.

Information on the above aspects may be communicated to the Editor.

Dr. G.V. Subba Rao
E-mail: phyvsg@nus.edu.sg

The Editorial Board of 'MRS-S OUTLOOK' reserves the right to include or not any of the submitted contributions.



Design & Typeset by Research Publishing Services
E-mail: enquiries@researchpubonline.com